

Hexoctahedral Au Nanocrystals with High-Index Facets and Their Optical and Surface-Enhanced Raman Scattering Properties

Jong Wook Hong, Su-Un Lee, Young Wook Lee, and Sang Woo Han*

Department of Chemistry and KI for the NanoCentury, KAIST, Daejeon 305-701, Korea

 Supporting Information

ABSTRACT: Au nanocrystals (NCs) with an unprecedented hexoctahedral structure enclosed exclusively by high-index {321} facets have been prepared for the first time. Manipulating the NC growth kinetics by controlling the amount of reductant and the reaction temperature in the presence of a suitable surfactant was the key synthetic lever for controlling the morphology of the Au NCs. The hexoctahedral Au NCs exhibited efficient optical and surface-enhanced Raman scattering activities due to their unique morphological characteristics.

Precise tuning of exposed facets on the surface of metal nanocrystals (NCs) by manipulation of the NC shape has provoked increasing research interest, as the inherent characteristics of NCs ranging from catalytic function to plasmonic properties strongly depend on their surface atomic arrangement.¹ During the past decade, the preparation and characterization of myriad shapes of mono- or multicomponent NCs have been reported.^{2,3} However, most of the synthesized NCs have been enclosed by low-index facets, such as {111}, {100}, and {110}, to minimize the surface energy during the course of NC growth. In recent years, the synthesis of high-index-faceted NCs has attracted a great deal of attention. High-index facets consist of surface atoms with lower coordination numbers than those of low-index facets due to the presence of high-density atomic steps and kinks on them. As such, their surface atoms have higher energy than those of low-index facets.⁴ Because of this high surface energy, high-index-faceted NCs have shown greatly enhanced performance for specific catalytic reactions relative to NCs bound by low-index facets. For example, Tian et al.⁵ reported that tetrahedrahedral (THH) Pt NCs with high-index {730} facets exhibited higher catalytic activity than NCs with low-index facets toward the electro-oxidation of formic acid and ethanol. Concave Pt NCs having high-index {411} facets also showed enhanced electrocatalytic activities compared with Pt/C and Pt black.⁶ In addition, monometallic Au and Pd NCs and Au–Pd bimetallic NCs with concave,⁷ THH,⁸ and trisoctahedral (TOH)⁹ shapes exhibited catalytic activities superior to those of low-index-faceted NCs. Very recently, efficient surface-enhanced Raman scattering (SERS) activities of high-index-faceted NCs, such as THH and elongated THH Au NCs and concave TOH Ag NCs, have also been reported.^{10,11} The pronounced SERS efficiencies have been attributed to the presence of large numbers of well-defined tips and edges in high-index-faceted NCs, which can serve as hot

spots for large electric-field enhancement and thus give strong SERS signals.

Among various high-index-faceted NCs, hexoctahedral (HOH) NCs, which are bounded by 48 triangular high-index {*hkl*} ($h > k > l > 0$) facets, are thought to be very promising nanomaterials for a range of applications because they are rich in energetic sites, including tips, edges, and intraparticle gaps.^{4b,9b} Additionally, HOH NCs contain not only steps but also kinks on their surfaces; thus, they have a higher surface energy than other NCs with stepped surfaces, such as THH, TOH, and concave polyhedral NCs. In this regard, HOH NCs composed of optically active materials such as Au and Ag are expected to show highly efficient plasmonic properties. However, the synthesis and characterization of HOH Au or Ag NCs have rarely been explored to date, although there have been very few limited successes in the preparation of Pt- and Pd-based HOH NCs through electrochemical and wet-chemical methods.^{4b,12} This may be due to the formidable difficulties in controlling such high-energy surfaces during the synthesis of NCs.

In this work, we present the first synthesis of HOH Au NCs enclosed exclusively by high-index {321} facets. To produce NCs with high-index facets, rational control of the NC growth kinetics is indispensable. The introduction of proper materials, such as specific surfactants or additional elements like foreign metal ions, which can stabilize high-index facets by adsorbing on the NC surfaces, can also play an essential role in the formation of high-index-faceted NCs.¹³ On the basis of these facts, we tried to synthesize HOH Au NCs by employing a high molar concentration of the reductant ascorbic acid (AA), a high reaction temperature for the fast reduction of the Au precursors, and cetyltrimethylammonium chloride (CTAC) as a surfactant. This led to the successful preparation of HOH Au NCs with high-index {321} facets. The plasmonic properties and SERS activities of the synthesized HOH Au NCs were also investigated.

The preparation of HOH Au NCs was achieved by exploiting a seed-mediated method [see the experimental details in the Supporting Information (SI)]. In the first step, Au NC seeds (average particle size = 5 nm; Figure S1 in the SI) were prepared by adding HAuCl₄ and NaBH₄ to an aqueous solution of CTAC with vigorous stirring. In a standard synthesis of the HOH Au NCs, aqueous solutions of HAuCl₄ (2.0 mL, 5 mM), Au NC seeds (0.1 mL, 2.3 μM_{Au}), and AA (1.0 mL, 0.3 M) were mixed with an aqueous solution of CTAC (20 mL, 0.1

Received: January 18, 2012

Published: February 24, 2012



M), and the resultant solution was rapidly heated on a hot plate with a constant heating rate of $15\text{ }^{\circ}\text{C min}^{-1}$ until the solution began to boil. The heating of the solution was then stopped, and the solution was left undisturbed at room temperature for ~ 6 h. Figure 1a,b shows typical scanning electron microscopy

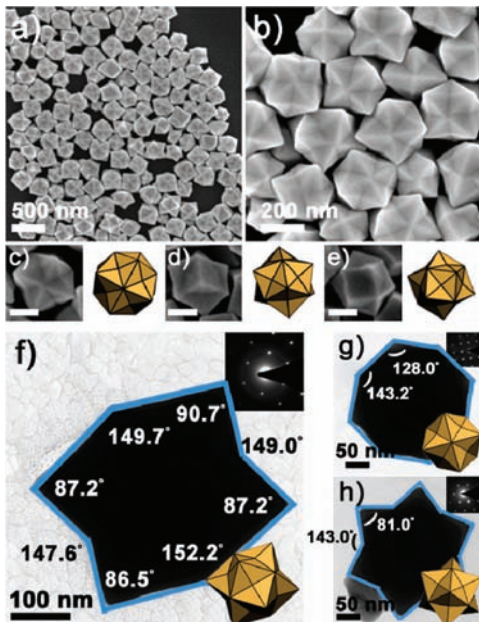


Figure 1. (a, b) SEM images of the HOH Au NCs. (c–e) SEM images and corresponding geometric models of NCs in different orientations. The scale bars indicate 150 nm. (f–g) TEM images and (insets) corresponding SAED patterns and structural models of the HOH Au NCs viewed along the (f) [110], (g) [100], and (h) [111] directions.

(SEM) images of the product, demonstrating the formation of high-purity (>90%) HOH Au NCs with an average NC size of 250 nm. High-magnification SEM images of NCs viewed along the different directions also showed that the NC shape closely matched the corresponding geometric models of hexoctahedra with different orientations (Figure 1c–e). To gain more detailed structural information, transmission electron microscopy (TEM) images of the HOH Au NCs viewed along the various directions were obtained. Figure 1f shows a TEM image of an individual HOH NC recorded along the [110] direction, as confirmed by the corresponding selected-area electron diffraction (SAED) pattern (Figure 1f inset). The Miller indices of high-index facets of NCs can be determined by using projection angles between edge-on facets of the NCs.¹⁴ From the comparison between the measured projection angles formed between edge-on facets (Figure 1f) and the calculated ones (Figure S2), the exposed facets of the prepared HOH Au NCs could be indexed as {321}. The TEM images of NCs recorded along the [100] and [111] directions and the corresponding SAED patterns also demonstrated that the synthesized NCs are enclosed predominantly by {321} facets (Figure 1g,h and Figure S3). The regular diffraction spots seen in the SAED patterns (Figure 1f–h insets) further confirmed the single-crystalline nature of the HOH Au NCs. The high-index {321} facets of the HOH Au NCs can be expressed in terms of a combination of low-index facets according to the microfacet notation¹⁵ as $[1_2(111) + 1_1(110) + 1_1(100)]$, implying the presence of (111) terraces with two unit cells, (110) steps with one unit cell, and (100) kinks with one unit

cell. The relative atomic sizes for the terraces, steps, and kinks are 2, 1, and 1, respectively. A high-resolution TEM (HRTEM) image and a three-dimensional lattice model of the {321} facets of the NCs are shown in Figure S4. Since the {321} facets of the Au NCs contain kinked steps, the Miller indices of their exposed surfaces could not be estimated from the atomic arrangement in the HRTEM images of the edge-on facets of NCs,^{9b,14b} as has been frequently done in the case of THH and TOH NCs with nonkinked steps to determine the type of exposed facets.

It is worth pointing out that the final morphology of the Au NCs strongly depended on the amount of HAuCl₄ added. The SEM images shown in Figure 2 demonstrate that various NCs

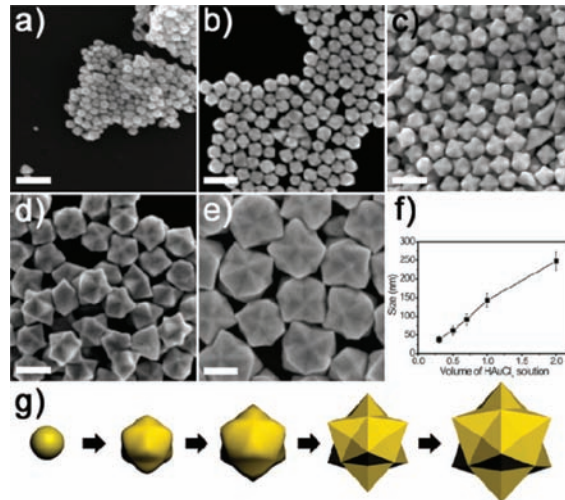


Figure 2. SEM images of the Au NCs prepared by using (a) 0.3, (b) 0.5, (c) 0.7, (d) 1.0, and (e) 2.0 mL of 5 mM HAuCl₄ solution. The scale bars indicate 200 nm. (f) Changes in NC size with increasing amount of HAuCl₄. (g) Scheme showing the shape evolution of the NCs.

are formed using different amounts of HAuCl₄ under otherwise identical synthetic conditions. When 0.3 mL of an aqueous solution of HAuCl₄ (5 mM) was employed in the synthesis instead of 2.0 mL as used in the standard procedure, roughly spherical Au NCs with an average diameter of 38 nm were produced (Figure 2a). Increasing the amount of HAuCl₄ solution to 0.5 mL yielded quasi-HOH NCs with an average size of 62 nm, which have a rudimentary structure of a hexoctahedron with rounded corners (Figure 2b). When the amount of HAuCl₄ solution was further increased to 0.7 mL, the NCs grew in size (average NC size = 92 nm) and had more resolved corners and edges than those prepared with 0.5 mL of HAuCl₄ solution (Figure 2c). As the amount of HAuCl₄ increased further, well-developed HOH NCs formed (Figure 2d,e). HOH Au NCs with average sizes of 143 and 250 nm were obtained by employing 1.0 mL and 2.0 mL (standard protocol) of HAuCl₄ solution, respectively. By comparing the projection angles between edge-on facets measured in the TEM images of NCs (Figure S5) with the calculated values (Figure S2), we found that the Au NCs prepared with 0.5–1.0 mL of HAuCl₄ solution were also enclosed predominantly by high-index {321} facets. The changes in NC size with increasing the amount of HAuCl₄ are summarized in Figure 2f. From these experimental results, the structural evolution of the HOH Au NCs could be deduced. Initially, spherical Au NCs are grown

from the seeds, and these are in turn transformed into quasi-HOH NCs and finally into well-defined HOH NCs (Figure 2g).

The formation of HOH Au NCs is highly sensitive to the reaction temperature. For instance, Au NCs generated by heating the reaction solution (at a constant heating rate of $15\text{ }^{\circ}\text{C min}^{-1}$) from room temperature up to 35 or $70\text{ }^{\circ}\text{C}$ (instead of $100\text{ }^{\circ}\text{C}$ as in the standard procedure) had irregular morphology or TOH structure, respectively (Figure S6a,b). These findings unambiguously reveal that a high reaction temperature is indispensable for the realization of HOH NCs. However, the use of a high temperature from the beginning of the reaction could reduce the stability of Au NC seeds, resulting in the low-yield ($\sim 25\%$) production of HOH Au NCs. Injection of HAuCl_4 , Au NC seeds, and AA into an aqueous solution of CTAC that had been preheated to $100\text{ }^{\circ}\text{C}$ did not yield high-purity HOH Au NCs (Figure S6c). Increasing the heating rate to a higher value ($20\text{ }^{\circ}\text{C min}^{-1}$) had no influence on the successful formation of $\{321\}$ -faceted HOH NCs (Figure S7). To validate further the importance of kinetic control in the synthesis of HOH Au NCs, the amount of reductant, AA, was varied during the synthesis, while the other experimental conditions were retained. When 0.1 or 0.3 mL of an aqueous solution of AA (0.3 M) was used in the synthesis, HOH Au NCs were not generated; instead, ill-defined polyhedral NCs with rounded edges were formed (Figure S8a,b). HOH Au NCs were obtained by increasing the amount of AA solution to 0.5 mL, which is half the amount used in the standard procedure; however, the yield was somewhat low ($\sim 75\%$) (Figure S8c). High yields of HOH Au NCs were produced only from reaction solutions containing AA in an amount larger than 1.0 mL (Figure 1 and Figure S8d). The presence of Cl^- ions was also crucial for the successful formation of HOH Au NCs. In fact, HOH NCs were not produced when CTAC molecules were replaced with cetyltrimethylammonium bromide (CTAB), which has the same CTA⁺ cation as CTAC (Figure S9a). This can be ascribed to the modulation of the reduction kinetics during the reaction. The Au precursor, AuCl_4^- , is converted to $[\text{AuCl}_{4-x}\text{Br}_x]^-$ in the presence of excess CTAB by a ligand exchange reaction. As the standard reduction potential of AuBr_4^- [0.854 V vs standard hydrogen electrode (SHE)] is lower than that of AuCl_4^- (1.002 V vs SHE),¹⁶ the reduction rate of the Au precursor is retarded. This was further confirmed by the fact that HOH NCs were not obtained when NaAuBr_4 was used as the Au precursor instead of HAuCl_4 (Figure S9b). These results of control experiments collectively demonstrated that manipulation of the growth kinetics of NCs by controlling the reaction temperature and the relative amount of AA as well as employing the proper surfactant is the key synthetic lever for controlling the final morphology of the Au NCs. Our findings imply that fast reduction kinetics can facilitate the formation of high-index-faceted HOH Au NCs.

Au NCs prepared with various amounts of HAuCl_4 were characterized by UV-vis spectroscopy (Figure 3a). The UV-vis extinction spectrum of the 38 nm spherical Au NCs obtained using 0.3 mL of HAuCl_4 solution showed a single surface plasmon resonance (SPR) peak at 537 nm, which can be assigned to the dipolar plasmon resonance of Au NCs. As the Au NCs grew in size, the maximum peak position of the dipolar SPR gradually red-shifted from 537 to 570 nm (62 nm quasi-HOH Au NCs) and then to 600 nm (92 nm quasi-HOH Au NCs). Interestingly, a shoulder peak at 568 nm first appeared

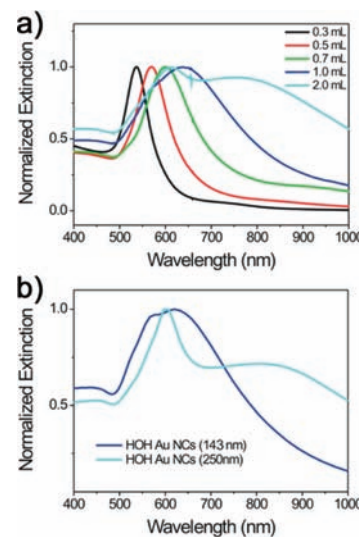


Figure 3. (a) Normalized UV-vis extinction spectra of Au NCs prepared with different amounts of HAuCl_4 . (b) FDTD-simulated extinction spectra of HOH Au NCs with average sizes of 143 and 250 nm.

nm in the extinction spectrum of the 143 nm HOH Au NCs, along with a strong red-shifted peak at 637 nm. These two peaks were further red-shifted as the size of the HOH Au NCs increased to 250 nm and split into two separate peaks at 613 and 753 nm. To gain more insight into the SPR characteristics of the HOH Au NCs, the optical properties of the NCs were computed using the finite-difference time domain (FDTD) method.¹⁷ The simulated extinction spectra of 143 and 250 nm HOH Au NCs (Figure 3b) correlate reasonably well with the experimental results. The SPR peaks observed at longer and shorter wavelengths for each HOH NC could be assigned to dipole and quadrupole plasmon modes, respectively, on the basis of FDTD-simulated phase images (Figure S10).

As mentioned above, the HOH Au NCs were expected to exhibit efficient SERS activity due to the presence of a large number of hot spots, such as well-defined tips, edges, and intraparticle gaps as well as high-energy step and kink atoms on their surfaces. Indeed, the FDTD-simulated electric field amplitude ($|E|$) distributions of the 250 nm HOH Au NCs with excitation wavelengths of $\lambda_{\text{ex}} = 632.8\text{ nm}$ showed much stronger (~ 100 -fold) field localizations at the NC vertexes relative to a spherical NC of similar size (230 nm) (Figure 4a–e). To investigate the SERS efficiency of the HOH Au NCs, we obtained SERS spectra of 4-nitrobenzenethiol (4-NBT) and 1,4-phenylenediisocyanide (1,4-PDI) adsorbed on the 250 nm HOH Au NCs with $\lambda_{\text{ex}} = 632.8\text{ nm}$. For comparison, SERS spectra of these molecules adsorbed on spherical Au NCs with a similar particle size ($\sim 230\text{ nm}$; Figure S11) were also obtained. The UV-vis spectral features of the spherical Au NCs were similar with those of the HOH Au NCs (Figure S12), ruling out a possible effect on SERS activity due to the degree of overlap between the SPR peak of the NCs and the excitation source. All of the SERS spectra were recorded from aqueous solutions with identical NC concentrations. The concentration of analyte was adjusted to be $1 \times 10^{-4}\text{ M}$. We obtained >10 SERS spectra for each sample, and averaged SERS spectra were then used for this study. As we expected, the HOH Au NCs gave stronger SERS signals than the spherical Au NCs (Figure 4f,g). The SERS intensities of 4-NBT and 1,4-

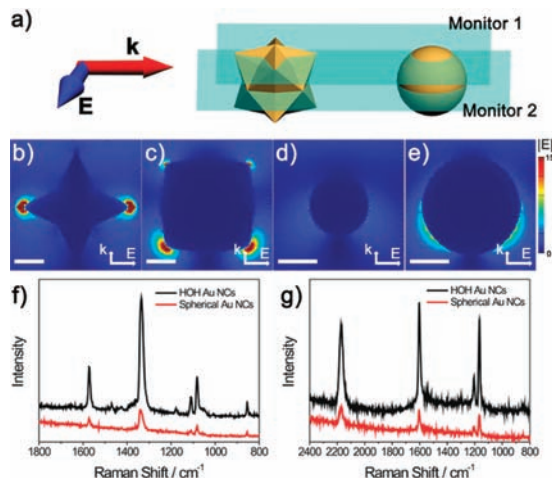


Figure 4. (a) FDTD-simulation models for calculating the $|E|$ distributions of the 250 nm HOH Au NCs and 230 nm spherical Au NCs. (b–e) $|E|$ distributions of the (b, c) HOH and (d, e) spherical Au NCs. The scale bars indicate 100 nm. $|E|$ distributions of the frequency-domain field profile are shown for (b, d) the monitor 1 plane and (c, e) the monitor 2 plane. (f, g) SERS spectra of (f) 4-NBT and (g) 1,4-PDI obtained with both the HOH Au NCs (black) and spherical Au NCs (red).

PDI molecules adsorbed on the HOH NCs were, respectively, 5.6 and 4.9 times higher than those adsorbed on the spherical NCs. From comparisons of the Raman spectra of aqueous solutions of 1,4-PDI and 4-NBT (0.1 M), we could estimate the enhancement factors of the HOH Au NCs to be 5.12×10^4 and 4.43×10^4 for 1,4-PDI and 4-NBT, respectively. Furthermore, SERS measurements on drop-cast films of the NCs on Si substrates showed results similar to those obtained in solution (Figure S13). These results indicate that efficient SERS activity benefits greatly from the unique morphological characteristics of the HOH Au NCs.

In summary, we have successfully synthesized HOH Au NCs bound by high-index {321} facets in aqueous solution. The presence of Cl^- ions, a high reaction temperature, and a high molar concentration of AA are critical for the formation of HOH Au NCs, revealing the importance of controlling the NC growth kinetics to achieve the production of this unique structure. HOH Au NCs exhibited enhanced plasmonic properties and higher SERS activities than low-index-faceted Au NCs. We expect that the exposed high-index surfaces of the NCs will promote their potential plasmonic and catalytic applications.

ASSOCIATED CONTENT

Supporting Information

Experimental details and additional data. This material is available free of charge via the Internet at <http://pubs.acs.org>.

AUTHOR INFORMATION

Corresponding Author

sangwoohahn@kaist.ac.kr

Notes

The authors declare no competing financial interest.

ACKNOWLEDGMENTS

This work was supported by Basic Science Research Programs (2010-0029149), the EPB Center (2008-0062042), and the

Future-Based Technology Development Program (Nano Fields) (2009-0082640) through the National Research Foundation (NRF) funded by the Korean Government (MEST) and was also supported by the Industrial Core Technology Development Program of the Ministry of Knowledge Economy (10037397). We thank D.-S. Kim and Professor Z. H. Kim for assistance with the FDTD simulations.

REFERENCES

- (a) Stamenkovic, V. R.; Fowler, B.; Mun, B. S.; Wang, G.; Ross, P. N.; Lucas, C. A.; Markovic, N. M. *Science* **2007**, *315*, 493.
- (b) Kondo, S.; Nakamura, M.; Maki, N.; Hoshi, N. *J. Phys. Chem. C* **2009**, *113*, 12625. (c) Yin, A.-X.; Min, X.-Q.; Zhang, Y.-W.; Yan, C.-H. *J. Am. Chem. Soc.* **2011**, *133*, 3816.
- (2) (a) Xia, Y.; Xiong, Y.; Lim, B.; Skrabalak, S. E. *Angew. Chem., Int. Ed.* **2009**, *48*, 60. (b) Jeong, G. H.; Kim, M.; Lee, Y. W.; Choi, W.; Oh, W. T.; Park, Q.-H.; Han, S. W. *J. Am. Chem. Soc.* **2009**, *131*, 1672.
- (c) Personick, M. L.; Langille, M. R.; Zhang, J.; Harris, N.; Schatz, G. C.; Mirkin, C. A. *J. Am. Chem. Soc.* **2011**, *133*, 6170. (d) Huang, X.; Tang, S.; Yang, J.; Tan, Y.; Zheng, N. *J. Am. Chem. Soc.* **2011**, *133*, 15946. (e) Chiu, C.-Y.; Li, Y.; Ruan, L.; Ye, X.; Murray, C. B.; Huang, Y. *Nat. Chem.* **2011**, *3*, 393.
- (3) (a) Habas, S. E.; Lee, H.; Radmilovic, V.; Somorjai, G. A.; Yang, P. *Nat. Mater.* **2007**, *6*, 692. (b) Zhang, J.; Fang, J. *J. Am. Chem. Soc.* **2009**, *131*, 18543. (c) Hong, J. W.; Lee, Y. W.; Kim, M.; Kang, S. W.; Han, S. W. *Chem. Commun.* **2011**, *47*, 2553. (d) Peng, Z.; You, H.; Yang, H. *ACS Nano* **2010**, *4*, 1501. (e) Lee, Y. W.; Kim, M.; Kang, S. W.; Han, S. W. *Angew. Chem., Int. Ed.* **2011**, *50*, 3466.
- (4) (a) Xiong, Y.; Wiley, B. J.; Xia, Y. *Angew. Chem., Int. Ed.* **2007**, *46*, 7157. (b) Tian, N.; Zhou, Z.-Y.; Sun, S.-G. *J. Phys. Chem. C* **2008**, *112*, 19801.
- (5) Tian, N.; Zhou, Z.-Y.; Sun, S.-G.; Ding, Y.; Wang, Z. L. *Science* **2007**, *316*, 732.
- (6) Huang, X.; Zhao, Z.; Fan, J.; Tan, Y.; Zheng, N. *J. Am. Chem. Soc.* **2011**, *133*, 4718.
- (7) (a) Zhang, J.; Langille, M. R.; Personick, M. L.; Zhang, K.; Li, S.; Mirkin, C. A. *J. Am. Chem. Soc.* **2010**, *132*, 14012. (b) Jin, M.; Zhang, H.; Xie, Z.; Xia, Y. *Angew. Chem., Int. Ed.* **2011**, *50*, 785.
- (8) (a) Ming, T.; Feng, W.; Tang, Q.; Wang, F.; Sun, L.; Wang, J.; Yan, C. *J. Am. Chem. Soc.* **2009**, *131*, 16350. (b) Tian, N.; Zhou, Z.-Y.; Yu, N.-F.; Wang, L.-Y.; Sun, S.-G. *J. Am. Chem. Soc.* **2010**, *132*, 7580. (c) Wang, F.; Li, C.; Sun, L.-D.; Wu, H.; Ming, T.; Wang, J.; Yu, J. C.; Yan, C.-H. *J. Am. Chem. Soc.* **2011**, *133*, 1106. (d) Lu, C.-L.; Prasad, K. S.; Wu, H.-L.; Ho, J. A.; Huang, M. H. *J. Am. Chem. Soc.* **2010**, *132*, 14546.
- (9) (a) Ma, Y.; Kuang, Q.; Jiang, Z.; Xie, Z.; Huang, R.; Zheng, L. *Angew. Chem., Int. Ed.* **2008**, *47*, 8901. (b) Yu, Y.; Zhang, Q.; Liu, B.; Lee, J. Y. *J. Am. Chem. Soc.* **2010**, *132*, 18258.
- (10) Yin, P.-G.; You, T.-T.; Tan, E.-Z.; Li, J.; Lang, X.-F.; Jiang, L.; Guo, L. *J. Phys. Chem. C* **2011**, *115*, 18061.
- (11) Xia, X.; Zeng, J.; McDearmon, B.; Zheng, Y.; Li, Q.; Xia, Y. *Angew. Chem., Int. Ed.* **2011**, *50*, 12542.
- (12) Zhang, L.; Zhang, J.; Kuang, Q.; Xie, S.; Jiang, Z.; Xie, Z.; Zheng, L. *J. Am. Chem. Soc.* **2011**, *133*, 17114.
- (13) (a) Yu, Y.; Zhang, Q.; Lu, X.; Lee, J. Y. *J. Phys. Chem. C* **2010**, *114*, 11119. (b) Personick, M. L.; Langille, M. R.; Zhang, J.; Mirkin, C. A. *Nano Lett.* **2011**, *11*, 3394.
- (14) (a) Zhou, K.; Li, Y. *Angew. Chem., Int. Ed.* **2012**, *51*, 602. (b) Kim, D.; Lee, Y. W.; Lee, S. B.; Han, S. W. *Angew. Chem., Int. Ed.* **2012**, *51*, 159.
- (15) Vanhove, M. A.; Somorjai, G. A. *Surf. Sci.* **1980**, *92*, 489.
- (16) CRC Handbook of Chemistry and Physics, 84th ed.; CRC Press: Boca Raton, FL, 2004; pp 8-29–8-30.
- (17) (a) Kim, D.-S.; Heo, J.; Ahn, S.-H.; Han, S. W.; Yun, W. S.; Kim, Z. H. *Nano Lett.* **2009**, *9*, 3619. (b) Lee, Y. W.; Kim, M.; Kim, Z. H.; Han, S. W. *J. Am. Chem. Soc.* **2009**, *131*, 17036.